

Molecular beam epitaxy of boron doped p-type BaSi₂ epitaxial films on Si(111) substrates for thin-film solar cells

著者別名	都甲 薫, 末益 崇
journal or publication title	Journal of crystal growth
volume	378
page range	201-204
year	2013-09
権利	(C) 2013 Elsevier B.V. NOTICE: this is the author ' s version of a work that was accepted for publication in Journal of crystal growth. Changes resulting from the publishing process, such as peer review, editing, corrections, structural formatting, and other quality control mechanisms may not be reflected in this document. Changes may have been made to this work since it was submitted for publication. A definitive version was subsequently published in Journal of crystal growth, 378, 2013 http://dx.doi.org/10.1016/j.jcrysgr.2012.12.153
URL	http://hdl.handle.net/2241/119793

doi: 10.1016/j.jcrysgr.2012.12.153

1 **Molecular beam epitaxy of boron doped p -type BaSi₂ epitaxial films on**
2 **Si(111) substrates for thin-film solar cells**

3

4 M. Ajmal Khan,^a Kosuke O. Hara,^b Kotaro Nakamura,^a Weijie Du,^a Masakazu Baba,^a
5 Katsuaki Toh,^a Mitsushi Suzuno,^a Kaoru Toko,^a Noritaka Usami,^{b,c} and
6 Takashi Suemasu^{a,c}

7

8 ^a*Institute of Applied Physics, University of Tsukuba, Tsukuba, Ibaraki 305-8573, Japan*

9 ^b*Institute for Materials Research, Tohoku University, Sendai, Miyagi 980-8577, Japan*

10 ^c*Japan Science and Technology Agency, CREST, Chiyoda, Tokyo 102-0075, Japan*

11

12 **Corresponding author:** Prof. T. Suemasu

13 Institute of Applied Physics, University of Tsukuba, Tsukuba, Ibaraki 305-8573, Japan

14 TEL/FAX: +81-29-853-5111, Email: suemasu@bk.tsukuba.ac.jp

15

16

17 **Abstract**

18 We have successfully grown *a*-axis-oriented *p*-type BaSi₂ films on Si(111) by *in situ* boron
19 (B) doping using molecular beam epitaxy (MBE). The hole concentration in B-doped BaSi₂
20 was controlled in the range between 10¹⁷ and 10¹⁹ cm⁻³ at room temperature by changing the
21 temperature of the B Knudsen cell crucible. The acceptor level was estimated to be
22 approximately 23 meV.

23

24

25 PACS: 78.40.Fy

26

27 **Keywords:** B1. semiconducting silicides; B2. BaSi₂; B3. solar cell; A3. MBE; A1. impurity
28 doping

29

30 **1. Introduction**

31 It is important for solar cell materials to have a large absorption coefficient and a
32 suitable band gap to yield high conversion efficiency. Materials that are composed of
33 abundant and non-toxic elements are also desirable. Among such materials we have focused
34 on semiconducting BaSi₂. The BaSi₂ has the orthorhombic lattice (space group Pnma) with a
35 unit cell containing 8 Ba and 16 Si atoms, the latter of which form Si₄ tetrahedra and can thus
36 be considered as Zintl phase [1,2]. Semiconducting BaSi₂ has the indirect band gap of
37 approximately 1.3 eV matching the solar spectrum and has a very large absorption coefficient
38 of $3 \times 10^4 \text{ cm}^{-1}$ at 1.5 eV [3-5]. Optical absorption measurements have shown that the band gap
39 of BaSi₂ can be increased up to 1.4 eV by replacing half of the Ba atoms in BaSi₂ with
40 isoelectric Sr atoms [6], which is in agreement with the theoretical calculations [7-9].
41 Recently, we successfully achieved large photoresponsivity and internal quantum efficiency
42 exceeding 70% in *a*-axis-oriented BaSi₂ epitaxial layers grown by molecular beam epitaxy
43 (MBE) [10-13]. These results have spurred interest in this material. The basic structure of a
44 solar cell is a *p-n* junction. Therefore, control of the conductivity of BaSi₂ by impurity doping
45 is a requirement. The carrier concentration of undoped *n*-BaSi₂ is approximately $5 \times 10^{15} \text{ cm}^{-3}$
46 [4]. According to Imai and Watanabe [14,15], substitution of Si in the BaSi₂ lattice is more
47 favorable than substitution of Ba from an energetic point of view by first-principles
48 calculation. In our previous works, the electron concentration of Sb-doped BaSi₂ was

49 controlled in the range between 10^{16} and 10^{20} cm^{-3} at room temperature (RT). In contrast, Al-
50 and In-doped BaSi_2 show p -type conductivity, but the hole concentration was limited up to
51 3×10^{17} cm^{-3} [16-19]. Thus, it is highly required to find another impurity atom for heavily
52 p -type doping of BaSi_2 . In this article, we chose to adopt boron (B) as an alternative impurity
53 and aimed to achieve p -type doping of over 10^{19} cm^{-3} in BaSi_2 films by MBE.

54

55 **2. Experimental**

56 Details of the growth procedure for *in situ* impurity doped BaSi_2 films have been previously
57 described for In- and Sb-doped BaSi_2 [17]. An ion-pumped MBE system equipped with
58 standard Knudsen cells (K-cells) for Ba and B, and an electron-beam evaporation source for
59 Si was used. For electrical measurements, high-resistivity floating-zone (FZ) n -Si(111) ($\rho >$
60 1000 $\Omega\cdot\text{cm}$) substrates were used. Briefly, MBE growth of B-doped BaSi_2 films was carried
61 out as follows. Firstly, a 10-nm-thick BaSi_2 epitaxial film was grown on Si(111) at 600 $^\circ\text{C}$ by
62 reactive deposition epitaxy (RDE; Ba deposition on a hot Si substrate), and this was used as a
63 template for the BaSi_2 overlayers. Next, Ba, Si, and B were co-evaporated at 600 $^\circ\text{C}$ onto the
64 BaSi_2 template to form impurity-doped BaSi_2 by MBE. The thickness of the grown layers
65 including the template was approximately 200-250 nm. The temperature of B, T_B , was varied
66 from 1250 to 1575 $^\circ\text{C}$ in samples A-G. The deposition rates of Si and Ba were approximately
67 1.5 and 4.0 nm/min, respectively. Sample preparation was summarized in Table 1. It turned

68 out that it was difficult to make ohmic contacts with Au/Cr on as-grown B-doped BaSi₂ films
69 for samples grown at $T_B \leq 1500^\circ\text{C}$. Thus rapid thermal annealing (RTA) was performed at
70 800 °C for 30 s in an Ar atmosphere with heating rate of 40°C/s for (samples C-G) prior to the
71 deposition of Au/Cr electrodes.

72 The crystal quality of the already grown layers was characterized by X-ray diffraction
73 (XRD) and reflection high-energy electron diffraction (RHEED) measurements. The electrical
74 properties were characterized by Hall measurements using the van der Pauw method. The
75 applied magnetic field was 0.5–0.7 T, normal to the sample surface. Secondary ion mass
76 spectroscopy (SIMS) measurements using O ions were performed to investigate the depth
77 profile of B doped. Reference samples with a controlled number of B atoms doped in BaSi₂
78 have not yet been prepared but will be necessary to precisely determine the impurity
79 concentration by SIMS.

80

81 **3. Results and discussion**

82 Figure 1 shows the θ -2 θ XRD patterns of B-doped as-grown BaSi₂ films with
83 $T_B = 1250\text{--}1575^\circ\text{C}$. The diffraction peaks of (100)-oriented BaSi₂, such as (200), (400) and
84 (600), are dominant in the θ -2 θ XRD patterns. These peaks match the epitaxial relationship
85 between BaSi₂ and Si. The forbidden diffraction peak designated by (*) is considered to be
86 due to double diffraction. Further increase of T_B resulted in two new diffraction peaks of

87 rhombohedral B(110) around $2\theta=36^\circ$ and B(220) at $2\theta=77^\circ$. This means that the crystalline
88 quality starts to deteriorate with increasing the amount of B atoms in the BaSi₂ films. Figures
89 2(a)-2(h) present the streaky RHEED patterns of B-doped as-grown BaSi₂ films prepared with
90 $T_B=1250-1575^\circ\text{C}$, respectively, observed along the Si[11-2] azimuth, indicating that the
91 BaSi₂ films were grown successfully. Figs. 3(a) and 3(b) show the SIMS depth profiles of B
92 concentration N_B in the B-doped as-grown BaSi₂ films prepared with $T_B=1450$ and 1550°C ,
93 respectively. The doped B atoms are uniformly distributed in the grown layers in both samples,
94 and they did not show any diffusion tendency. Similar results were also obtained in other
95 samples. The averaged value of N_B for BaSi₂ prepared with $T_B=1450^\circ\text{C}$ is approximately
96 $2\times 10^{21}\text{ cm}^{-3}$ in Fig. 3(a), while that with $T_B=1550^\circ\text{C}$ is $1\times 10^{22}\text{ cm}^{-3}$ in Fig. 3(b). This result is
97 explained relatively well by the difference in vapor pressure of B; The vapor pressure of B at
98 1550°C is approximately 7 times larger than that at 1450°C [20]. These results mean that the
99 concentration of B atoms in the BaSi₂ can be controlled by T_B . The B concentrations in the
100 SIMS profiles shown in Fig. 3 were corrected using reference samples, where controlled
101 number of B atoms was doped in the BaSi₂ films by ion implantations. The activation rate of
102 B atoms can be thus estimated, that is approximately $p=10^{19}\text{ cm}^{-3}/N_B=10^{22}\text{ cm}^{-3}\cong 0.1\%$ for
103 sample H. But it was found from plan-view transmission electron microscopy images and also
104 from the θ - 2θ XRD patterns that some amounts of B atoms were in the form of B clusters.
105 Thus the actual B activation rate in the BaSi₂ film is supposed to be much higher than the

106 above value of 0.1%, and it is approximately 1% for sample H. The reason of such a small
107 activation rate of B is probably attributed to relatively low growth temperature of 600°C and
108 too much B concentrations.

109 We next move on to the electrical properties of B-doped as-grown BaSi₂ films,
110 samples H and I. The hole concentration p was 1.0×10^{19} for sample H, and $2.5 \times 10^{18} \text{ cm}^{-3}$ for
111 sample I at RT. These values are the highest ever reported for p -type BaSi₂. We speculate that
112 defects induced by crystallized B in the BaSi₂ film could cause the reduced p in sample I. In
113 order to evaluate the acceptor level E_A in sample H, we performed the temperature
114 dependence of p . To secure the ohmic contacts on the surface at lower temperatures, first the
115 temperature dependence of current-voltage (I - V) characteristics were measured as shown in
116 Fig. 4(a). Ohmic behavior was confirmed over the wide temperature range between 30 and
117 300 K. Resistance increases with decreasing temperature in Fig. 4(a), which is typical for
118 semiconductors. Fig. 4(b) gives the temperature dependence of p for sample H. The acceptor
119 level calculated using Eq. (1) was about 23 meV.

$$120 \quad p \propto \exp\left(-\frac{E_A}{2k_B T}\right) \quad (1)$$

121 Here, k_B is the Boltzmann's constant, and T the absolute temperature. This E_A value is much
122 smaller than that in Al-doped BaSi₂ ($E_A=50$, and 140 meV) [18]. Such a shallow E_A level of
123 23 meV could be the reason for heavily p -type doping in sample H. Regarding the other
124 samples, it was difficult to obtain reliable hole concentration and mobility data at RT. Thus,

125 we performed the RTA treatment on samples C-I to achieve activation of doped B atoms. The
126 obtained p and hole mobility μ_h were summarized in Table 1. The hole concentration
127 increases gradually from 10^{17} to 10^{19} cm^{-3} with increasing T_B , thereby showing that the RTA is
128 a very effective means to activate the B atoms.

129 Figure 5 shows the measured μ_h versus p for B-doped BaSi_2 . As the hole
130 concentration increases the mobility decreases. This trend is usually predicted by ionized
131 impurity scattering in conventional semiconductors. The hole mobilities are always smaller
132 than the electron mobilities in Sb-doped BaSi_2 [17]. According to Migas *et al.*, this is
133 attributed to a larger effective mass for holes than electrons [3]. The p value reached a
134 maximum of 3.4×10^{19} cm^{-3} , and the resistivity was $0.02 \Omega \cdot \text{cm}$ in sample G. At present, only
135 limited information has been obtained for the electrical properties of B-doped BaSi_2 . We
136 speculate that both growth temperatures during MBE and RTA duration influence the
137 electrical properties of B-doped BaSi_2 . Thus, further studies are necessary in order to optimize
138 the growth condition for B-doped BaSi_2 films by MBE.

139

140 **4. Conclusions**

141 We achieved the hole concentration of over 10^{19} cm^{-3} at RT in *in situ* B-doped BaSi_2
142 films by MBE. The acceptor level was estimated to be approximately 23 meV from the
143 temperature dependence of hole concentration. The RTA treatment performed at 800 °C for

144 30 s in Ar activated the B atoms in the BaSi₂ films. The hole concentration increased by the
145 RTA treatment and reached a maximum of $3.4 \times 10^{19} \text{ cm}^{-3}$ for BaSi₂ prepared with
146 $T_B = 1550 \text{ }^\circ\text{C}$.

147

148 **Acknowledgements**

149 The authors would like to thanks Prof. Tanimoto of the University of Tsukuba for his
150 kind help for XRD measurements, Dr. Imai of AIST for useful discussion. We would also like
151 to thank Dr. Mitsushi Suzuno for the helpful discussions and valuable comments during the
152 course of this research. This work was supported in part by Core Research for Evolutional
153 Science and Technology (CREST) of the Japan Science and Technology Agency.

154

155 **References**

- 156 [1] J. Evers, G. Oehlinger, A. Weiss, *Angew. Chem., Int. Ed.*, 16 (1977) 659.
- 157 [2] M. Imai, T. Hirano, *J. Alloys Compd.* 224 (1995) 111.
- 158 [3] D.B. Migas, V.L. Shaposhnikov, V.E. Borisenko, *Phys. Status Solidi B* 244 (2007) 2611.
- 159 [4] K. Morita, Y. Inomata, T. Suemasu, *Thin Solid Films* 508 (2006) 363.
- 160 [5] K. Toh, T. Saito, T. Suemasu, *Jpn. J. Appl. Phys.* 50 (2011) 068001.
- 161 [6] K. Morita, Y. Inomata, T. Suemasu, *Jpn. J. Appl. Phys.* 45 (2006) L390.
- 162 [7] Y. Imai, A. Watanabe, *Thin Solid Films* 515 (2007) 8219.
- 163 [8] Y. Imai, A. Watanabe, *Intermetallics* 18 (2010) 348.
- 164 [9] Y. Imai, A. Watanabe, *Intermetallics* 18 (2010) 1432.
- 165 [10] W. Du, M. Suzuno, M. A Khan, K. Toh, M. Baba, K. Nakamura, K. Toko, N. Usami, T.
166 Suemasu, *Appl. Phys. Lett.* 100 (2012) 152114.
- 167 [11] Y. Matsumoto, D. Tsukada, R. Sasaki, M. Takeishi, T. Suemasu, *Appl. Phys. Express* 2
168 (2009) 021101.
- 169 [12] D. Tsukada, Y. Matsumoto, R. Sasaki, M. Takeishi, T. Saito, N. Usami, T. Suemasu, *Appl.*
170 *Phys. Express* 2 (2009) 051601.
- 171 [13] T. Saito, Y. Matsumoto, M. Suzuno, M. Takeishi, R. Sasaki, N. Usami, T. Suemasu,
172 *Appl. Phys. Express* 3 (2009) 021301.
- 173 [14] Y. Imai, A. Watanabe, *Intermetallics* 15 (2007) 1291.

- 174 [15] Y. Imai, A. Watanabe, *Intermetallics* 19 (2011) 1102.
- 175 [16] M. Kobayashi, K. Morita, T. Suemasu, *Thin Solid Films* 515 (2007) 8242.
- 176 [17] M. Kobayashi, Y. Matsumoto, Y. Ichikawa, D. Tsukada, T. Suemasu, *Appl. Physics*
177 *Express* 1 (2008) 051403.
- 178 [18] M. Takeishi, Y. Matsumoto, R. Sasaki, T. Saito, T. Suemasu, *Physics Procedia* 11 (2011)
179 27.
- 180 [19] M. Ajmal Khan, M. Takeishi, Y. Matsumoto, T. Saito, and T. Suemasu, *Physics Procedia*
181 11 (2011) 11.
- 182 [20] D. Stull, *American Institute of Physics Handbook, Third Edition*, McGraw Hill, New
183 York, 1972.
- 184
- 185

186 **Figure Captions**

187

188 Fig. 1 θ - 2θ XRD patterns of B-doped BaSi₂ films grown at $T_B=1250$ - 1575 °C.

189

190 Fig. 2 RHEED patterns of B-doped BaSi₂ films when T_B is (a) 1250, (b) 1300, (c) 1350, (d)
191 1400, (e) 1450, (f) 1500, (g) 1550, and (h) 1575 °C, observed along the Si[11-2] azimuth.

192

193 Fig. 3. SIMS profiles of B for BaSi₂ films grown at $T_B=(a)$ 1450 and (b) 1550 °C.

194

195 Fig. 4. Temperature dependence of (a) I - V characteristics and (b) p for B-doped as-grown
196 BaSi₂ films grown with $T_B=1550$ °C (sample G).

197

198 Fig. 5. Relationship of measured μ_h versus p for B-doped BaSi₂ films at RT.

199

200

201

202

203

204 Table 1 Sample preparation: B temperature, annealing temperature and duration during RTA,
 205 measured hole concentration and mobility are shown.

206

207	Sample	T_B	RTA	p	μ_p
208		(°C)		(cm ⁻³)	(cm ² /V·s)
209	A	1250	w/o	-	-
210					
211	B	1300	w/o	-	-
212					
213	C	1350	800 °C /30 s	8.5×10^{16}	23
214					
215	D	1400	800 °C /30 s	1.2×10^{17}	168
216					
217	E	1450	800 °C /30 s	5.0×10^{17}	59
218					
219	F	1500	800 °C /30 s	5.2×10^{17}	17
220					
221	G	1550	800 °C /30 s	3.4×10^{19}	8.3
222					
223	H	1550	w/o	1.0×10^{19}	6.3
224					
225	I	1575	w/o	2.5×10^{18}	8.3
226					

227

228

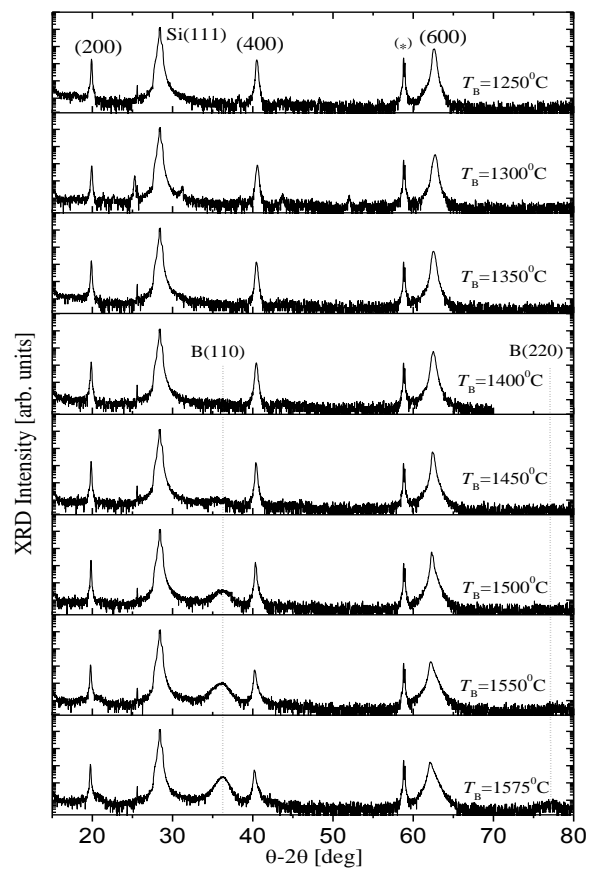


Fig. 1

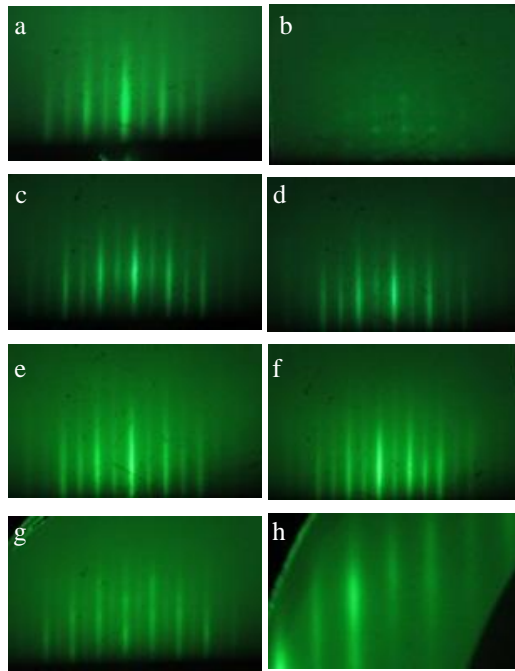


Fig. 2

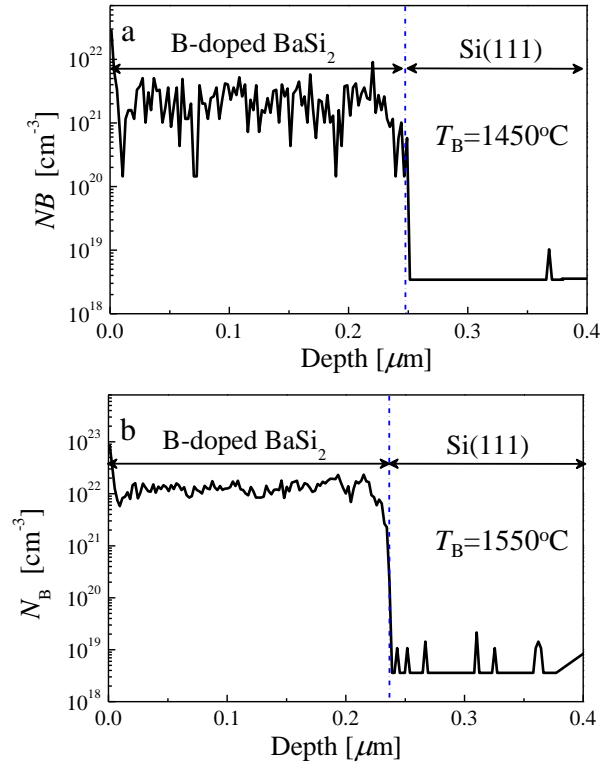


Fig. 3

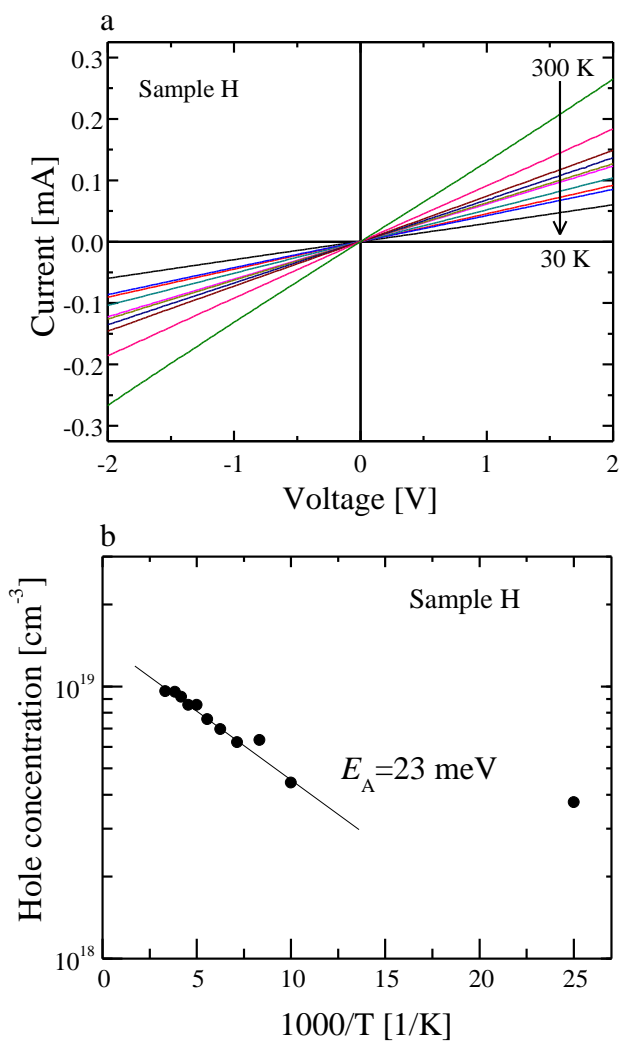


Fig. 4

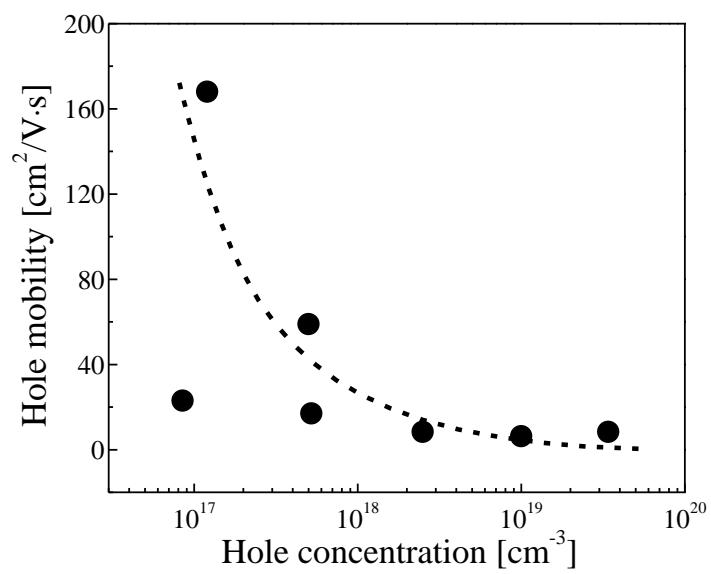


Fig. 5